Surface and interface states of Bi2Se3 thin films investigated by optical second-harmonic generation and terahertz emission

S. Y. Hamh, S.-H. Park, S.-K. Jerng, J. H. Jeon, S. H. Chun, J. H. Jeon, S. J. Kahng, K. Yu, E. J. Choi, S. Kim, S.-H. Choi, N. Bansal, S. Oh, Joonbum Park, Byung-Woo Kho, Jun Sung Kim, and J. S. Lee

Articles you may be interested in

Aging and reduced bulk conductance in thin films of the topological insulator Bi2Se3
J. Appl. Phys. 113, 153702 (2013); 10.1063/1.4801911

Modulation of external electric field on surface states of topological insulator Bi2Se3 thin films
Appl. Phys. Lett. 101, 223109 (2012); 10.1063/1.4767998

Significant second-harmonic generation in two lead-free polar oxides BiInO 3 and BiAlO 3 : A first-principles investigation
Appl. Phys. Lett. 94, 191908 (2009); 10.1063/1.3136838

Spectroscopic second harmonic generation measured on plasma-deposited hydrogenated amorphous silicon thin films
Appl. Phys. Lett. 85, 4049 (2004); 10.1063/1.1812836

Second-harmonic generation study of domain walls in x Bi 2 Ti 4 O 11 -(1−x) Bi 4 Ti 3 O 12 films with large dielectric permittivity
J. Appl. Phys. 91, 3172 (2002); 10.1063/1.1445497
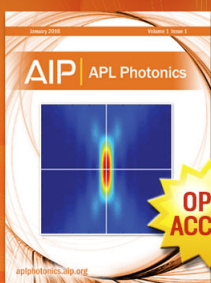
Surface and interface states of Bi₂Se₃ thin films investigated by optical second-harmonic generation and terahertz emission

S. Y. Hamh,[1] S.-H. Park,[1] S.-K. Jerng,[2] J. H. Jeon,[2] S. H. Chun,[2] J. H. Jeon,[3] S. J. Kahng,[3]
K. Yu,[4] E. J. Choi,[4] S. Kim,[5] S.-H. Choi,[5] N. Bansal,[6] S. Oh,[7] Joonbum Park,[8]
Byung-Woo Kho,[8] Jun Sung Kim,[8] and J. S. Lee[1,a)]

[1]*Department of Physics and Photon Science, School of Physics and Chemistry, Gwangju Institute of Science and Technology, Gwangju 500-712, Korea*
[2]*Department of Physics and Graphene Research Institute, Sejong University, Seoul 143-747, Korea*
[3]*Department of Physics, Korea University, Seoul 136-701, Korea*
[4]*Department of Physics, University or Seoul, Seoul 130-743, Korea*
[5]*Department of Applied Physics, College of Applied Science, Kyung Hee University, Yongin 446-701, Korea*
[6]*Department of Electrical and Computer Engineering, Rutgers, The state University of New Jersey, Piscataway, New Jersey 08854, USA*
[7]*Department of Physics and Astronomy, Rutgers, The state University of New Jersey, Piscataway, New Jersey 08854, USA*
[8]*Department of Physics, Pohang University of Science and Technology, Pohang 790-784, Korea*

We investigate the surface and interface states of Bi₂Se₃ thin films by using the second-harmonic generation technique. Distinct from the surface of bulk crystals, the film surface and interface show the isotropic azimuth dependence of second-harmonic intensity, which is attributed to the formation of randomly oriented domains on the in-plane. Based on the nonlinear susceptibility deduced from the model fitting, we determine that the surface band bending induced in a space charge region occurs more strongly at the film interface facing the Al₂O₃ substrate or capping layer compared with the interface facing the air. We demonstrate that distinct behavior of the terahertz electric field emitted from the samples can provide further information about the surface electronic state of Bi₂Se₃. © *2016 AIP Publishing LLC*. [http://dx.doi.org/10.1063/1.4941420]

The surface state of topological insulators (TIs) has attracted significant attention because it provides a topologically protected and spin-polarized Dirac band; thus, it can serve as a platform for spintronic applications.[1–6] In particular, thin-film TIs have been highlighted to reduce the bulk carrier effect and also to exploit the surface charge transport due to their large surface-to-volume ratio. The Dirac dispersion of the surface state and the corresponding carrier dynamics were examined by using angle-resolved photoemission and terahertz (THz) spectroscopy, respectively.[2–4,7–10] In such TIs prepared in the thin-film form, top and bottom interfaces can have distinct electronic behavior, as they face the air and the substrate, for example. Although the Dirac nature of the interface electronic state was examined through tunneling spectroscopy in a TI/non-TI p–n junction, it is generally difficult to examine the electronic properties of the bottom interface compared with the top surface.[11]

As a lowest-order-nonlinear-optical process, second-harmonic generation (SHG) can provide valuable information about the surface state of TIs. Second-harmonic (SH) light is generated only in a region with broken inversion symmetry. Since TIs, such as Bi₂Se₃, are centrosymmetric, the SHG process takes place only at its surface with longitudinal field discontinuity and in the space charge region with a built-in electric field. Azimuth-dependent SH intensity for the Bi₂Se₃ single crystal revealed the crystal symmetry and the time evolution of the space charge region after the cleavage of the sample.[12,13] Additionally, an attempt was made to

understand the spin-momentum-locked state by activating the SHG process with circularly polarized light.[12,13]

In this paper, we investigate the interface electronic states of Bi₂Se₃ films as well as their surface states by using the SHG technique. We observe the isotropic azimuth dependence of the SH intensity for Bi₂Se₃ films, which we attribute to the signature of the multi-domain formation at both the top surface and the bottom interface of films. Furthermore, we determine part of the second-order susceptibility tensor components from the model fitting of SHG responses and demonstrate that the symmetry breaking is stronger near the interface facing the Al₂O₃ layer than the interface facing the air. We also demonstrate that THz emission spectroscopy can provide complimentary information about the surface electronic state of Bi₂Se₃ thin films.

Bi₂Se₃ films were fabricated by using commercial molecular beam epitaxy equipment. The substrates used for the film growth are non-crystalline Si nanocrystals (Si NCs)/Si and crystalline Al₂O₃.[14–18] For the Si NCs/Si substrate, SiO$_x$/SiO₂ multilayers were grown on Si wafers through ion beam sputtering and subsequently annealed to form Si NCs, and then 30-nm-thick Bi₂Se₃ was grown.[14–16,18] For the film grown on Al₂O₃, one sample was left with Bi₂Se₃ as a top surface, and the other sample was capped with a 20-nm-thick Al₂O₃ layer via atomic layer deposition. In the former and latter cases, the Bi₂Se₃ film thicknesses were about 30 and 20 nm, respectively. Figure 1(a) shows the x-ray diffraction patterns of Bi₂Se₃ films grown on Si NCs/Si (black) and Al₂O₃ without (red) and with (blue) the capping layer. They exhibit diffraction peaks corresponding to (003)-type lattice
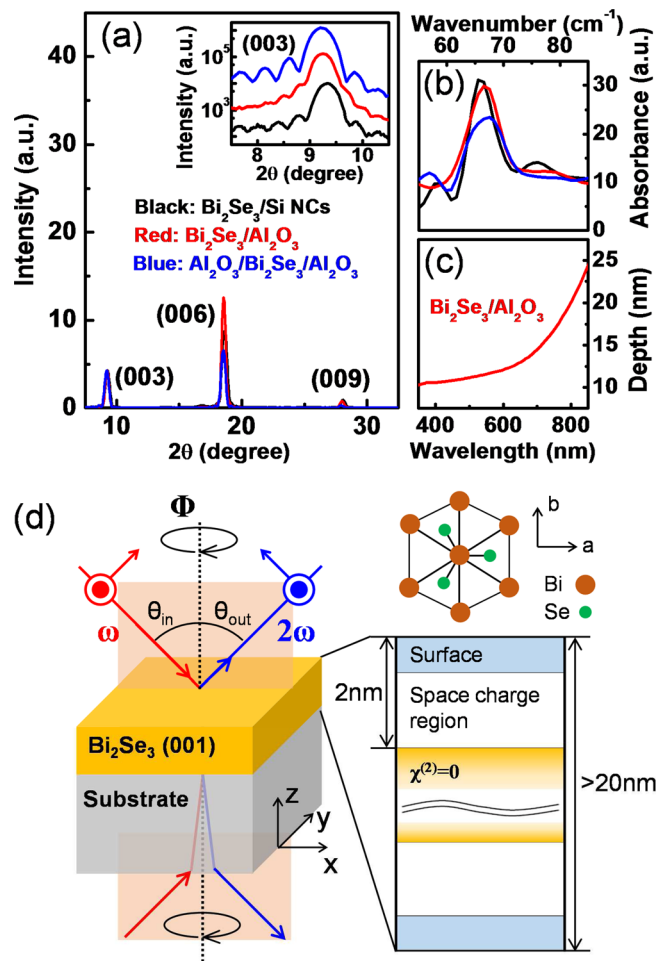
a)Electronic mail: jsl@gist.ac.kr

FIG. 1. (a) X-ray diffraction peaks of Bi_2Se_3 films. Inset displays an enlarged (003) peak that clearly shows an interference fringe. (b) Absorbance spectra where a transverse optic phonon mode appears as a peak structure at around 65 cm^{-1}. (c) Penetration depth of incident light to Bi_2Se_3 thin film. (d) Scheme of second-harmonic generation (SHG) experiment and SHG active regions in the Bi_2Se_3 film.

planes and well-defined fringe oscillation around the Bragg peak (inset), which are indicative of an epitaxial growth of the film along the c-axis. Figure 1(b) displays absorbance spectra where a transverse-optic phonon mode appears as a peak structure at around 65 cm^{-1}, which is in close agreement with the reported value of the bulk Bi_2Se_3.[19] Films with smaller thicknesses down to 6 nm were prepared, and structural characterization revealed that they have comparable crystallinity compared with thick films. For the comparison, we prepared a single crystal of Bi_2Se_3 by using a flux method. All the samples were kept in the air for more than one week before the measurement so that the surface state of Bi_2Se_3 could interact sufficiently with an atmospheric environment.[20–22]

We used an 800-nm wavelength wave (ω) as fundamental light and detected 400-nm wavelength SH light (2ω) in a specular-reflection geometry in which the incident and detection angles (θ_{in} and θ_{out}, respectively) were 45° from the surface normal, as shown in Fig. 1(d). Laser pulses of about 100-fs duration and an 80-MHz repetition rate illuminated the sample with a power density of about 0.1 kW/cm^2, which is lower than the damage threshold.[12,13] We employed a short-pass filter and a band-pass filter to isolate the SH light

emitted from the sample and detected the SH light intensity by using a photomultiplier tube with full variations of input and output polarization as well as the sample azimuth Φ.

The SHG response can be a direct probe of the symmetry breaking selectively at the surface or at the interface depending on the optical geometry. In Bi_2Se_3 films, the interface and the space charge layer, as shown in Fig. 1(d), are the SHG active parts, whereas the inner region is SHG-inactive, as it is centrosymmetric. This SHG-active region is about 2-nm thick.[12] Considering that the penetration depths of light with the wavelengths of 800 and 400 nm are around 20 and 10 nm, respectively (Fig. 1(c)),[13] the 20 and 30-nm-thick films allow a separate probe of surface and interface states by illuminating light from the top and the bottom sides, respectively, and detecting SH light in a backward geometry, as depicted in Fig. 1(d). Note that Al_2O_3 is transparent in near-infrared and visible spectral regions, including the wavelengths of 800 and 400 nm, and gives negligible SH intensity.

Figures 2(a)–2(d) display Φ-dependent SH light intensities $I(2\omega)$ for one single crystal and the other three thin films of Bi_2Se_3. All the results were obtained in a $S_{in}P_{out}$ geometry (i.e., with S-polarized fundamental light and P-polarized SH light). The bulk Bi_2Se_3 shows a three-fold symmetry, which is a typical 3m point group response
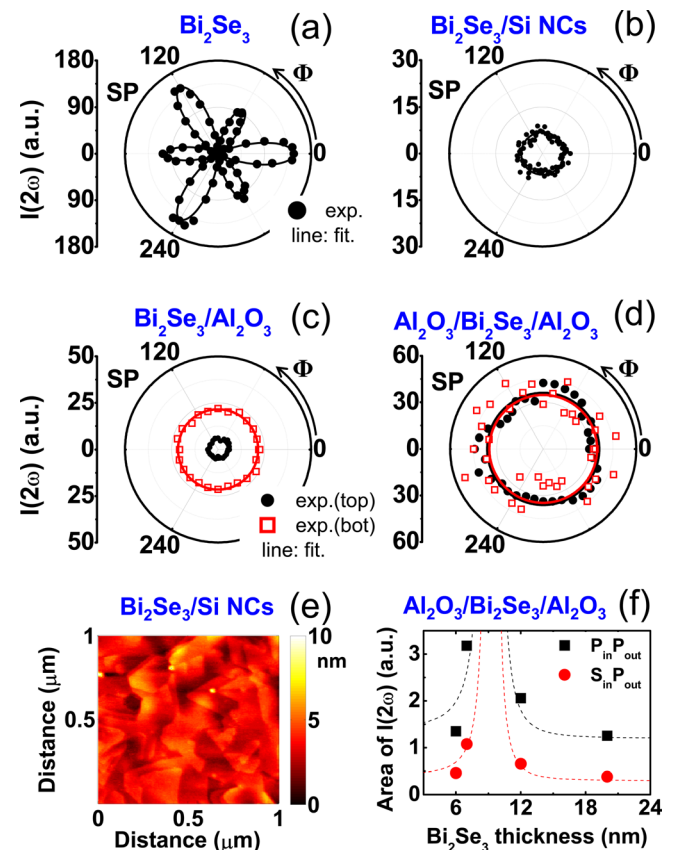

FIG. 2. (a)–(d) Second-harmonic (SH) light intensity $I(2\omega)$ as function of azimuth angle Φ. SP indicates S- and P-polarization of fundamental and SH light, respectively. (e) Atomic force microscopy image of Bi_2Se_3 films grown on Si NCs/Si. (f) Thickness dependence of $I(2\omega)$ integrated over Φ. Dotted lines are drawn by considering contributions from capacitor-type dc electric-field and Lorentz-type resonance near 9 nm to $I(2\omega)$ in thin films (Ref. 26).

(Fig. 2(a)).[12] On the other hand, $I(2\omega)$ from all three films are finite but unchanged upon the variation of Φ, as shown in Figs. 2(b)–2(d). A similar isotropic SH response is observed for a $P_{in}P_{out}$ geometry, whereas $I(2\omega)$ is almost negligible for the $S_{in}S_{out}$ and $P_{in}S_{out}$ geometries (not shown).

Although such behavior of $I(2\omega)$ for the films is reminiscent of the 4 mm point group, we attribute it instead to the formation of the domains with random in-plane orientations;[17,18,23–25] this can make the in-plane SH response effectively inversion-symmetric, whereas the inversion symmetry along the out-of-plane direction remains broken. In this context, it is straightforward to understand not only the isotropic SHG responses for P_{out} geometries but also the negligible $I(2\omega)$ for S_{out} geometries. The formation of multi-domains is confirmed from the atomic force microscopy images taken for Bi_2Se_3/Si NCs (Fig. 2(e)) and Bi_2Se_3/Al_2O_3 (not shown). It should be noted that the bottom interface of Bi_2Se_3 grown on Al_2O_3 exhibited essentially the same isotropic behavior of SH responses (open squares in Fig. 2(c)). Therefore, we suppose that similar domains would also be formed at the film–substrate interface.

Recently, Glinka *et al.* reported the SHG responses of thin-film TIs with various thicknesses, which showed a clear three-fold symmetry at least for the samples with a thickness of up to 20 nm.[26] Such distinct SHG responses between the previous report and this work are attributable to the distribution of domains; supposing that a nonlinear medium is inhomogeneous, $I(2\omega)$ should depend strongly on the length scale of the inhomogeneity and the spatial coherence of fundament light. Nevertheless, it is worth noting that the thickness-dependent $I(2\omega)$ exhibits similar behavior to the results in Ref. 26 (Fig. 2(f)).

For the more quantitative analysis, we modeled the induced SH polarization $P(2\omega)$ as a linear summation of the contributions from each domain as $P(2\omega) = f \times P_1(2\omega) + (1-f) \times P_2(2\omega)$. Here, f and $(1-f)$ mean the volume fractions of domains 1 and 2, respectively. In the $S_{in}P_{out}$ configuration, the Φ-dependent $P(2\omega)$ is described in the case of the 3m point group as $P_i^{S_{in}P_{out}}(2\omega) = c_i^{(1)}\cos(3\Phi)a_i^{(1)} + c_i^{(2)}a_i^{(2)}$ with $i = 1$ or 2.[13] $c_i^{(1)}$ and $c_i^{(2)}$ are constants determined by Fresnel equations with consideration of multiple reflections as, for example, $0.0001 + 0.0178i$ and $0.0455 - 0.0279i$, respectively, for the surface facing the air. $a_i^{(1)}$ and $a_i^{(2)}$ are defined as an addition of second- and third-order susceptibilities with the same symmetry (i.e., $a_i^{(1)} = \chi_{xxx} + \chi_{xxxz}$ and $a_i^{(2)} = \chi_{zxx} + \chi_{zxxz}$).[13] For the multi-domains, we assume that there always exist domains with opposite in-plane orientations, and consequently, all the in-plane components will be cancelled out. Hence, the polarization formula is changed to $P^{S_{in}P_{out}}(2\omega) = c^{(2)}a^{(2)}$. Here, the subscript for denoting the domain is not used anymore. We fit the experimental data with $I(2\omega) \propto |P(2\omega)|^2$, as shown by the solid lines in Fig. 2. (The results in Fig. 2(d) have finite three-fold modulation, but we traced the median level to estimate the $a^{(2)}$ value.) For the bulk sample, we first determined $a^{(1)}$ by fitting $I(2\omega)$ in the $S_{in}S_{out}$ configuration as $P^{S_{in}S_{out}}(2\omega) = c^{(3)}\sin(3\Phi)a^{(1)}$ with $c^{(3)}$ determined by the

Fresnel equation and then obtained $a^{(2)}$ from $I(2\omega)$ in the $S_{in}P_{out}$ configuration using the aforementioned equation.[13]

By investigating the details of fitting parameters, we discuss the degree of inversion symmetry breaking for the film surfaces and interfaces. Figure 3 shows $|a^{(2)}|$ values obtained for the Bi_2Se_3 bulk and thin films. All the quantities are normalized to the value of the bulk sample. Filled circles and open squares denote parameters for the top and the bottom Bi_2Se_3 interfaces, respectively. Interestingly, all the surfaces facing the air have comparable values of $|a^{(2)}|$ irrespective of the sample types or substrates used for the film growth. It is worth emphasizing that the value of the interface facing the Al_2O_3 layer is larger by about four times than those of the interfaces between Bi_2Se_3 and air. This demonstrates that the inversion symmetry is broken more strongly in the former case than the latter.

Since the SHG can occur at the surface itself or in the space charge region, it is unclear which one has the dominant contribution to the larger symmetry breaking at the Bi_2Se_3-Al_2O_3 interface; accordingly, a complexity arises in the interpretation of the SHG results. Concerning the relative phase of each contribution to the total SH intensity, on the other hand, we can obtain a useful hint from a report by Hsieh *et al.* for the Bi_2Se_3 single crystal; the time-dependent $I(2\omega)$ shows a monotonic increase after the sample cleavage.[12,13] Since the downward band bending progresses due to the Se vacancy, this suggests that the surface charge discontinuity and the downward band bending have the same phase in their contributions to SHG. Note that the charge discontinuity is expected to be less for the Al_2O_3–Bi_2Se_3 interface than for the air–Bi_2Se_3 interface. Therefore, the larger
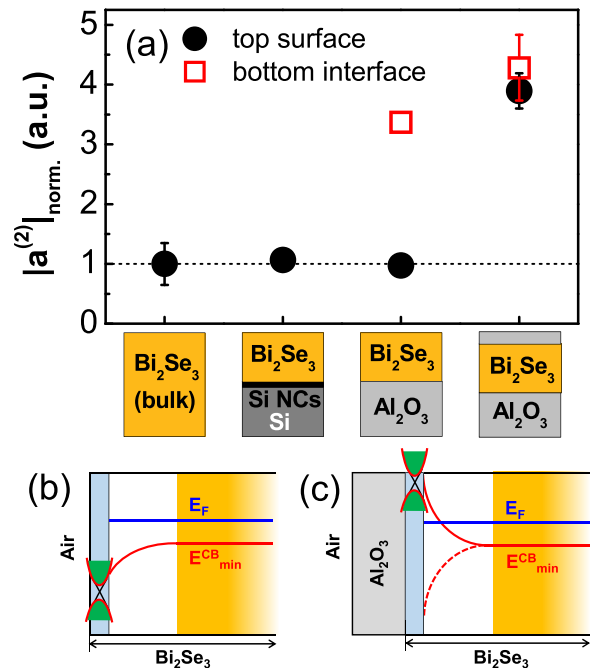

FIG. 3. (a) Sample-dependent second-order nonlinear tensor component $|a^{(2)}|$ normalized to value for bulk Bi_2Se_3. (b) and (c) Schematics of surface band bending of Bi_2Se_3 facing the air and Al_2O_3, respectively. Region in light blue (orange) indicates surface (bulk) state. E_F and E^{CB}_{min} represent Fermi energy and conduction band minimum, respectively. Dotted and solid lines in (c) display two possible band bending states at Bi_2Se_3 interface facing Al_2O_3.

$|a^{(2)}|$ for the Al_2O_3–Bi_2Se_3 interface compared with that of the air–Bi_2Se_3 interface is attributable to the larger contribution of surface band bending. This interpretation is further reinforced if we assume the destructive contribution of the charge discontinuity against surface band bending. Figures 3(b) and 3(c) depict possible surface electronic states of Bi_2Se_3 facing the air and Al_2O_3, respectively. Here, the air–Bi_2Se_3 interface is considered to have downward bend bending,[4,12,13,27] and the Al_2O_3–Bi_2Se_3 interface provides stronger band bending although its direction has not been determined yet.

As a second probe of the surface electronic states, THz emission arising from the photo-carrier acceleration or optical rectification is examined. Similarly with the SHG experiment, a THz wave can be generated near the surface upon its illumination with infrared laser pulses (Fig. 4(a)). The emitted THz wave is guided by a set of parabolic mirrors, and its transient electric field profiles are detected by a photoconductive antenna.[28,29] The time-profiles of the THz electric field emitted from the top surfaces of Bi_2Se_3 are displayed in Fig. 4(b). Except for the Bi_2Se_3 film grown on Al_2O_3 without the capping layer, the THz electric field exhibits isotropic behavior upon the variation of Φ (not shown).[9,29] This leads us to exclude optical rectification as a possible mechanism of the THz emission and to consider the surge current mechanism as a primary emission source of the THz emission from Bi_2Se_3. Upon the formation of photo-excited carriers, a transient electric dipole-generating THz wave is formed by a mobility difference between an electron and a hole (photo–Dember effect) or by a charge-acceleration due to a built-in field. We take the THz wave emitted from InAs as a reference waveform induced by the larger electron mobility than the hole (Fig. 4(b)).[30] When the photo-carriers are accelerated in upward (downward) band bending, the direction of the transient dipole, or equivalently the phase of the THz wave, will be the same as (opposite to) that formed in InAs.[31] Therefore, we determined the surface electronic states by examining the details of the THz field profiles, namely, the phase and amplitude of the emitted THz wave.

For Bi_2Se_3 facing the air, the phase of the THz wave is opposite to that of InAs (Fig. 4(b)). In a recent report by Luo *et al.*, however, the THz wave emitted from Bi_2Se_3 has the same phase as that of InAs.[9] These contrasting results imply that the THz phase is determined sensitively by the detailed balance between two competing contributions from the mobility difference and the band bending. In the case of the Bi_2Se_3 crystal studied in the present work, the opposite phase of the emitted THz wave compared with that of InAs is attributed to the fact that the dominant THz generation mechanism at the air–Bi_2Se_3 interface is downward band bending (Fig. 3(b)), which is in close agreement with the conventional understanding of the surface state of Bi_2Se_3.[4,12,13,27] In this way, when the THz wave has an opposite phase to that of InAs, the direction of the band bending can be clearly determined. However, the Bi_2Se_3 film surface facing Al_2O_3 is not straightforward, as the phase of the THz wave is the same as that of InAs. This implies two possible interpretations. Firstly, the surface facing Al_2O_3 would emit the THz wave mainly through the photo–Dember effect. Secondly, the surface state of Bi_2Se_3 may have upward band bending so that the photo–Dember effect and the band bending contribute constructively to the large THz field strength. To reach a clearer conclusion about the surface electronic state, additional efforts are desirable to separate the photo–Dember effect from THz emission processes.

In summary, we investigated the surface and interface states of Bi_2Se_3 thin films in the aspect of inversion symmetry breaking by employing SHG and THz emission techniques. We modeled the SHG process by considering the domains with random in-plane orientations to account for the isotropic azimuth dependence of the second-harmonic intensity and estimated part of the second-order-nonlinear susceptibility tensor components. Additionally, we examined electric-field profiles of emitted THz waves, which showed distinct behavior in their phases depending on the adjacent layer that the Bi_2Se_3 film faced. Based on these results, we suggested that inversion symmetry breaking occurs more strongly at the interface facing Al_2O_3 than that facing the air. The band bending formed in the space charge region can shift the location of the Fermi energy relative to the surface Dirac state, as depicted schematically in Figs. 3(b) and 3(c), which can determine the majority-carrier type of the surface state as well as the carrier number. Therefore, the transport properties of the interface/surface state of topological insulators can be controlled by choosing a proper substrate or capping layer, and interface-sensitive SHG and THz emission techniques can provide useful information about interface/surface electronic states that is otherwise difficult to obtain.
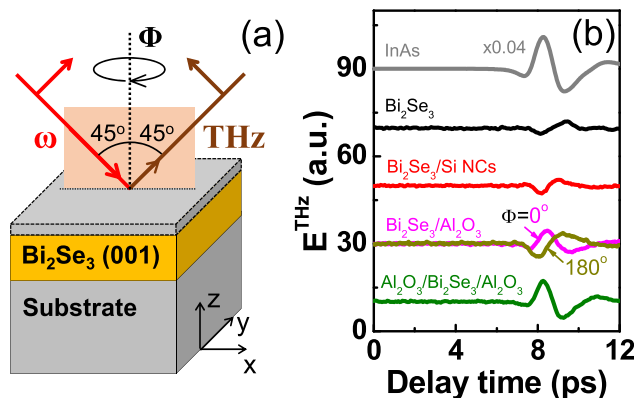
FIG. 4. (a) Schematic of terahertz (THz) emission experiment. (b) Time-profiles of THz electric field emitted from top surfaces of Bi_2Se_3 samples.

[1]L. Fu, C. L. Kane, and E. J. Mele, Phys. Rev. Lett. **98**, 106803 (2007).

[2]D. Hsieh, D. Qian, L. Wray, Y. Xia, Y. S. Hor, R. J. Cava, and M. Z. Hasan, Nature **452**, 970–974 (2008).

[3]D. Hsieh, Y. Xia, L. Wray, D. Qian, A. Pal, J. H. Dil, J. Osterwalder, F. Meier, G. Bihlmayer, C. L. Kane, Y. S. Hor, R. J. Cava, and M. Z. Hasan, Science **323**, 919–922 (2009).

[4]D. Hsieh, Y. Xia, D. Qian, L. Wray, J. H. Dil, F. Meier, J. Osterwalder, L. Patthey, J. G. Checkelsky, N. P. Ong, A. V. Fedorov, H. Lin, A. Bansil, D. Grauer, Y. S. Hor, R. J. Cava, and M. Z. Hasan, Nature **460**, 1101–1105 (2009).

[5]J. E. Moore, Nature **464**, 194–198 (2010).

[6]M. Z. Hasan and C. L. Kane, Rev. Mod. Phys. **82**, 3045 (2010).

[7]Y. Zhang, K. He, C. Z. Chang, C. L. Song, L. L. Wang, X. Chen, J. F. Jia, Z. Fang, X. Dai, W. Y. Shan, S. Q. Shen, Q. Niu, X. L. Qi, S. C. Zhang, X. C. Ma, and Q. K. Xue, Nat. Phys. **6**, 584–588 (2010).

[8]R. V. Aguilar, A. V. Stier, W. Liu, L. S. Bilbro, D. K. George, N. Bansal, L. Wu, J. Cerne, A. G. Markelz, S. Oh, and N. P. Armitage, Phys. Rev. Lett. **108**, 087403 (2012).

[9]C. W. Luo, H. J. Chen, C. M. Tu, C. C. Lee, S. A. Ku, W. Y. Tzeng, T. T. Yeh, M. C. Chiang, H. J. Wang, W. C. Chu, J. Y. Lin, K. H. Wu, J. Y. Juang, T. Kobayashi, C. M. Cheng, C. H. Chen, K. D. Tsuei, H. Berger, R. Sankar, F. C. Chou, and H. D. Yang, Adv. Opt. Mater. **1**(11), 804–808 (2013).

[10]B. C. Park, T.-H. Kim, K. I. Sim, B. Kang, J. W. Kim, B. Cho, K.-H. Jeong, M.-H. Cho, and J. H. Kim, Nat. Commun. **6**, 6552 (2015).

[11]R. Yoshimi, A. Tsukazaki, K. Kikutake, J. G. Checkelsky, K. S. Takahashi, M. Kawasaki, and Y. Tokura, Nat. Mater. **13**, 253–257 (2014).

[12]D. Hsieh, J. W. McIver, D. H. Torchinsky, D. R. Gardner, Y. S. Lee, and N. Gedik, Phys. Rev. Lett. **106**, 057401 (2011).

[13]J. W. McIver, D. Hsieh, S. G. Drapcho, D. H. Torchinsky, D. R. Gardner, Y. S. Lee, and N. Gedik, Phys. Rev. B **86**, 035327 (2012).

[14]N. Bansal, Y. S. Kim, E. Edrey, M. Brahlek, Y. Horibe, K. Iida, M. Tanimura, G. H. Li, T. Feng, H. D. Lee, T. Gustafsson, E. Andrei, and S. Oh, Thin Solid Films **520**, 224–229 (2011).

[15]K. J. Kim, D. W. Moon, S. H. Hong, S. H. Choi, M. S. Yang, J. H. Jhe, and J. H. Shin, Thin Solid Films **478**, 21–24 (2005).

[16]S. Kim, M. C. Kim, S. H. Choi, K. J. Kim, H. N. Hwang, and C. C. Hwang, Appl. Phys. Lett. **91**, 103113 (2007).

[17]S.-K. Jerng, K. Joo, Y. Kim, S.-M. Yoon, J. H. Lee, M. Kim, J. S. Kim, E. Yoon, S.-H. Chun, and Y. S. Kim, Nanoscale **5**, 10618 (2013).

[18]N. Bansal, N. Koirala, M. Brahlek, M.-G. Han, Y. Zhu, Y. Cao, J. Waugh, D. S. Dessau, and S. Oh, Appl. Phys. Lett. **104**, 241606 (2014).

[19]A. D. LaForge, A. Frenzel, B. C. Pursley, T. Lin, X. Liu, J. Shi, and D. N. Basov, Phys. Rev. B **81**, 125120 (2010).

[20]M. Brahlek, Y. S. Kim, N. Bansal, E. Edrey, and S. Oh, Appl. Phys. Lett. **99**, 012109 (2011).

[21]C. Chen, S. He, H. Weng, W. Zhang, L. Zhao, H. Liu, X. Jia, D. Mou, S. Liu, J. He, Y. Peng, Y. Feng, Z. Xie, G. Liu, X. Dong, J. Zhang, X. Wang, Q. Peng, Z. Wang, S. Zhang, F. Yang, C. Chen, Z. Xu, X. Dai, Z. Fang, and X. J. Zhou, Proc. Natl. Acad. Sci. U. S. A. **109**(10), 3694–3698 (2012).

[22]L. V. Yashina, J. Sanchez-Barriga, M. R. Scholz, A. A. Volykhov, A. P. Sirotina, V. S. Neudachina, M. E. Tamm, A. Varykhalov, D. Marchenko, G. Springholz, G. Bauer, A. Knop-Gericke, and O. Rader, ACS Nano **7**(6), 5181–5191 (2013).

[23]D. L. Medlin, Q. M. Ramasse, C. D. Spataru, and N. Y. C. Yang, J. Appl. Phys. **108**, 043517 (2010).

[24]N. V. Tarakina, S. Schreyeck, T. Borzenko, C. Schumacher, G. Karczewski, K. Brunner, C. Gould, H. Buhmann, and L. W. Molenkamp, Cryst. Growth Des. **12**(4), 1913–1918 (2012).

[25]S. Schreyeck, N. V. Tarakina, G. Karczewski, C. Schumacher, T. Borzenko, C. Brüne, H. Buhmann, C. Gould, K. Brunner, and L. W. Molenkamp, Appl. Phys. Lett. **102**, 041914 (2013).

[26]Y. D. Glinka, S. Babakiray, T. A. Jhnnson, M. B. Holcomb, and D. Lederman, Phys. Rev. B **91**, 195307 (2015).

[27]H.-J. Noh, H. Koh, S.-J. Oh, J.-H. Park, H.-D. Kim, J. D. Rameau, T. Valla, T. E. Kidd, P. D. Johnson, Y. Hu, and Q. Li, Europhys. Lett. **81**, 57006 (2008).

[28]J. W. Han, S. Y. Hamh, T. H. Kim, K. S. Lee, N. E. Yu, D.-K. Ko, and J. S. Lee, Opt. Lett. **39**(19), 5531–5534 (2014).

[29]The Bi_2Se_3 film grown on Al_2O_3 without the capping layer exhibits an anisotropic behaviour which was attributed to the vicinality of the substrate and inclined film surface. (S. Y. Hamh *et al.*, Nanoscale Res. Lett. **10**, 489 (2015).) We observed a similar anisotropic azimuth-dependence for the bottom interface formed between Bi_2Se_3 film and the Al_2O_3 substrate, and excluded it in the discussion.

[30]Y. B. Gao, B. He, D. Parker, I. Androulakis, and J. P. Heremans, Phys. Rev. B **90**, 125204 (2014).

[31]P. Gu, M. Tani, S. Kono, K. Sakai, and X. C. Zhang, J. Appl. Phys. **91**, 5533 (2002).